



UNIVERSITY OF LEEDS

This is a repository copy of *Optically pumped terahertz laser based on intersubband transitions in a GaN/AlGaIn double quantum well* .

White Rose Research Online URL for this paper:  
<http://eprints.whiterose.ac.uk/1118/>

---

**Article:**

Vukmirovic, N., Jovanovic, V.D., Indjin, D. et al. (3 more authors) (2005) Optically pumped terahertz laser based on intersubband transitions in a GaN/AlGaIn double quantum well. *Journal of Applied Physics*, 97 (10). 103106-(5 pages). ISSN 1089-7550

<https://doi.org/10.1063/1.1900929>

---

**Reuse**

See Attached

**Takedown**

If you consider content in White Rose Research Online to be in breach of UK law, please notify us by emailing [eprints@whiterose.ac.uk](mailto:eprints@whiterose.ac.uk) including the URL of the record and the reason for the withdrawal request.



[eprints@whiterose.ac.uk](mailto:eprints@whiterose.ac.uk)  
<https://eprints.whiterose.ac.uk/>



## White Rose Consortium ePrints Repository

<http://eprints.whiterose.ac.uk/>

This is an author produced version of a paper published in **Journal of Applied Physics**.

White Rose Repository URL for this paper:  
<http://eprints.whiterose.ac.uk/archive/00001118/>

---

### Published paper

Vukmirovic, N. and Jovanovic, V.D. and Indjin, D. and Ikonc, Z. and Harrison, P. and Milanovic, V. (2005) *Optically pumped terahertz laser based on intersubband transitions in a GaN/AlGaIn double quantum well*. Journal of Applied Physics, 97 (10). 103106-(5 pages).

### Repository paper

Vukmirovic, N. and Jovanovic, V.D. and Indjin, D. and Ikonc, Z. and Harrison, P. and Milanovic, V. (2005) *Optically pumped terahertz laser based on intersubband transitions in a GaN/AlGaIn double quantum well*.  
Author manuscript available at: <http://eprints.whiterose.ac.uk/archive/00001118/>

---

# Optically pumped terahertz laser based on intersubband transitions in a GaN/AlGaN double quantum well

N. Vukmirović, V. D. Jovanović, D. Indjin, Z. Ikonić, P. Harrison  
School of Electronic and Electrical Engineering, University of Leeds, Leeds  
LS2 9JT, United Kingdom

V. Milanović  
School of Electrical Engineering, Bulevar kralja Aleksandra 73, 11120  
Belgrade, Serbia and Montenegro

## Abstract

A design for a GaN/AlGaN optically pumped terahertz laser emitting at  $34\mu\text{m}$  ( $\Delta E \sim 36\text{ meV}$ ) is presented. The quasi-bound energies and associated wave functions are calculated with the intrinsic electric field induced by the piezoelectric and the spontaneous polarization. The structures based on a double quantum well were simulated and the output characteristics extracted using a fully self-consistent rate equation model with all relevant scattering processes included. Both electron-longitudinal optical phonon and electron acoustic phonon interactions were taken into account. A population inversion of 12% for a pumping flux  $\Phi = 10^{27}\text{ cm}^{-2}\text{s}^{-1}$  at room temperature was calculated. By comparing the calculated modal gain and estimated waveguide and mirror losses the feasibility of laser action up to room temperature is predicted.

## 1 Introduction

More than three decades have passed since the first proposal of a laser based on intersubband transitions in quantum wells [1]. Improvements in technology in the last decade have led to the realization of infrared intersubband lasers based on GaAs/AlGaAs and AlInAs/GaInAs and most recently on InAs/AlSb material systems. The electrically pumped or quantum cascade laser (QCL) from its first realization [2] has demonstrated an impressive and rapid development extending the emission wavelengths from the mid-infrared to the THz spectral range [3, 4, 5, 6, 7, 8, 9]. However, QCLs based on polar semiconductors such as GaAs/AlGaAs and AlInAs/GaInAs are not capable of emitting in the energy range around the longitudinal optical (LO) phonon energies ( $E_{LO} \sim 36\text{ meV}$  in GaAs and  $E_{LO} \sim 34\text{ meV}$  in InGaAs), leaving a gap in the spectral range between 30 and 40  $\mu\text{m}$ . In comparison with QCLs,

optically pumped intersubband lasers[10] have the disadvantage that an external pumping source is necessary. However, they offer the advantages of easier design and fabrication, higher selectivity in populating energy levels and a way of avoiding the free-carrier losses associated with contact regions.

Recently, intersubband transitions in GaN/AlGaN heterostructures started to attract the attention of researchers due to the prospect of their applications in optoelectronic devices. The large LO phonon energy and ultra-fast electron dynamics [11, 12, 13] offer a route for achieving the 30-40  $\mu\text{m}$  terahertz region as the corresponding intersubband transitions are not influenced by the resonant electron-LO phonon interactions like in GaAs based systems[14]. The first design and theoretical investigations of a terahertz GaN/AlGaN QCL emitting in GaAs Reststrahlenband has been presented recently [15].

In this paper we present a design and a simulation of a GaN/AlGaN-based optically pumped far-infrared (THz) intersubband laser, emitting in the GaAs forbidden Reststrahlenband at 34  $\mu\text{m}$  corresponding to a laser energy separation of 36 meV. A detailed investigation of the possible population inversion and calculation of the output characteristics of proposed structure is also presented.

## 2 Theoretical model

Consider a GaN/AlGaN multiple quantum well consisting of  $N$  layers with widths  $L_1, \dots, L_N$ , grown along the  $z$ -direction (Fig 1.). The envelope function Schrödinger equation in effective mass approximation, in a system where a strong intrinsic electric field exists, is given as[16]: (for in-plane wave vector  $k_{\parallel} = 0$ ):

$$-\frac{\hbar^2}{2} \frac{d}{dz} \left( \frac{1}{m(z)} \frac{d\eta}{dz} \right) + [x_i \Delta U + eF_i z + C_i] \eta(z) = E\eta(z), \quad (1)$$

where  $m(z)$  is the parabolic effective mass (note that nonparabolicity was disregarded as the energies of corresponding states in this particular - terahertz design were not far above the conduction band edge),  $\Delta U$  is the conduction band offset,  $F_i$  is the intrinsic polarization induced field in the  $i$ -th layer, and  $C_i = C_{i-1} + e(F_{i-1} - F_i)L_{i-1}$  with the arbitrary taken  $C_1 = 0$ . The polarization-induced electric fields have been calculated using the expression [17]

$$F_j = \frac{\sum_{k=1}^N (P_k - P_j) \frac{L_k}{\epsilon_k}}{\epsilon_j \sum_{k=1}^N \frac{L_k}{\epsilon_k}}, \quad (2)$$

where  $\varepsilon_i$  is the dielectric constant and  $P_i$  is the total polarization in  $i$ -th layer given as a sum of piezoelectric and spontaneous (pyroelectric) polarizations. The piezoelectric polarization was calculated as

$$P_{pz} = 2 \frac{a - a_k}{a_k} \left( e_{31} - e_{33} \frac{C_{13}}{C_{33}} \right), \quad (3)$$

where  $C_{ij}$  are elastic constants,  $e_{ij}$  are piezoelectric constants,  $a_k$  is the lattice constant of the  $k$ -th layer, and  $a$  is the lattice constant of the buffer. In order to provide pseudomorphic growth, the buffer lattice constant (Al content in the buffer layer) has been chosen to satisfy the strain-balancing condition as in Ref. [16].

The spontaneous polarization was calculated with the bowing factor included:

$$P_{sp} = x P_{sp}^{AlN} + (1 - x) P_{sp}^{GaN} - Cx(1 - x), \quad (4)$$

where  $x$  is the molar content of AlN in the layer,  $P_{sp}^{AlN} = -0.090$  C/m<sup>2</sup>,  $P_{sp}^{GaN} = -0.034$  C/m<sup>2</sup> and  $C = -0.021$  C/m<sup>2</sup> (see Ref. [18]).

Since  $m(z)$  is constant within a layer, an analytic treatment of equation (1) is possible. As the effective potential is stepwise linear, the two linearly independent solutions of the Schrödinger equation in each layer can be written in the form of Airy functions of the first and second kind[19].

## 2.1 Laser model

The rate equations for the three-level system were used to find the population inversion and the gain. These equations read:

$$\frac{dn_1}{dt} = -\sigma_{13}\Phi(n_1 - n_3) + W_{21}n_2 + W_{31}n_3 - W_{12}n_1 - W_{13}n_1, \quad (5)$$

$$\frac{dn_2}{dt} = W_{32}n_3 - W_{21}n_2 + W_{12}n_1 - W_{23}n_2, \quad (6)$$

$$\frac{dn_3}{dt} = \sigma_{13}\Phi(n_1 - n_3) - W_{31}n_3 - W_{32}n_3 + W_{13}n_1 + W_{23}n_2, \quad (7)$$

where  $n_i$ [cm<sup>-2</sup>] is the electron density in the  $i$ -th subband,  $\Phi$ [cm<sup>-2</sup>s<sup>-1</sup>] is the pump flux,  $W_{ij}$  are the transition rates between subbands and  $\sigma_{13}$  is the pump absorption cross section. The optical cross sections were calculated according to

$$\sigma_{if} = \frac{e^2 \omega \pi}{\bar{n} \varepsilon_0 c} z_{if}^2 \frac{2}{\pi \Gamma}, \quad (8)$$

where  $z_{if}$  is the dipole matrix element  $z_{if} = \int \eta_i^* z \eta_f dz$ ,  $\omega$  is the frequency of the transition,  $\bar{n}$  is the refractive index in the GaN/GaAlN alloy, and  $\Gamma$  the

transition linewidth. The transition linewidth was taken to be equal to 15% of the transition energy.

In the calculation of the transition rates, the processes of emission and absorption of polar optical phonons, as well as acoustic phonons, were taken into account. Bulk-like phonon modes were assumed.

The transition rate for scattering an electron from initial state in subband  $i$  with in-plane wave vector  $k_i$  into any state in subband  $f$  (assuming the final state is empty) via the interaction with LO phonon is given by [20]:

$$W_{if}^{LO\mp}(k_i) = \frac{\Upsilon''\pi}{2}\Theta(k_i^2 - \frac{2m\Delta}{\hbar^2}) \int_{-\infty}^{+\infty} \frac{|G_{if}(K_z)|^2 dK_z}{\sqrt{K_z^4 + 2K_z^2(2k_i^2 - \frac{2m\Delta}{\hbar^2}) + (\frac{2m\Delta}{\hbar^2})^2}} \quad (9)$$

where  $\Theta(x) = \begin{cases} 0 & x \leq 0 \\ 1 & x > 0 \end{cases}$  is the step function,  $\Upsilon'' = \frac{2m\epsilon^2\omega_{LO}P'}{\hbar^2}$ ,  $P' = (N_0 + \frac{1}{2} \mp \frac{1}{2}) (\frac{1}{\epsilon_\infty} - \frac{1}{\epsilon_0})$ , the sign - corresponds to absorption, and + to emission,  $\omega_{LO}$  is the LO phonon frequency,  $\Delta = E_{f0} - E_{i0} \mp \hbar\omega_{LO}$  (where  $E_{f0}$  and  $E_{i0}$  are energies of the bottoms of the subbands  $f$  and  $i$ , respectively),  $\epsilon_\infty$  is the high frequency dielectric constant,  $\epsilon_0$  static dielectric constant,  $N_0 = (\exp \frac{\hbar\omega_{LO}}{k_B T} - 1)^{-1}$  number of phonons with frequency  $\omega_{LO}$  at a temperature  $T$ , and  $G_{if}(K_z) = \int \eta_i(z)^* \exp(iK_z z) \eta_f(z) dz$  is the electron-phonon interaction form factor, while the transition rate for scattering via acoustic phonons is [20]:

$$W_{if}^{A\mp}(k_i) = \frac{D_A^2 m}{\rho v_s \hbar^2} \int_0^\infty dK_z \int_0^{2\pi} d\phi |G_{if}(K_z)|^2 \frac{f(\alpha_1) + f(\alpha_2)}{\alpha_1 - \alpha_2}, \quad (10)$$

where

$$f(\alpha) = \theta(\alpha) \alpha \sqrt{\alpha^2 + K_z^2} \left( N_0(\sqrt{\alpha^2 + K_z^2}) + \frac{1}{2} \mp \frac{1}{2} \right),$$

$N_0(K) = (\exp \frac{\hbar v_s K}{k_B T} - 1)^{-1}$ ,  $\alpha_{1,2} = -k_i \cos \phi \pm \sqrt{(k_i \cos \phi)^2 - \frac{2m\Delta}{\hbar^2}}$ ,  $\Delta = E_{f0} - E_{i0}$ ,  $D_A$  is the acoustic deformation potential,  $\rho$  the density, and  $v_s$  the longitudinal sound velocity. Equations (9) and (10) were derived under the assumption of parabolic subbands with the same effective mass  $m$ . This assumption will be justified later.

Transition rates calculated according to (9) and (10) were averaged across the subband with the effect of final-state blocking included, thus yielding:

$$\langle W_{if}^{LO\mp} \rangle = \frac{1}{2n_i \pi} \int_0^\infty d(k_i^2) W_{if}^{LO\mp}(k_i) f_{FD}(E_i(k_i), E_{Fi}) [1 - f_{FD}(E_i(k_i) \pm \hbar\omega, E_{Ff})], \quad (11)$$

$$\langle W_{if}^{A\mp} \rangle = \frac{1}{2n_i\pi} \int_0^\infty d(k_i^2) W_{if}^{A\mp}(k_i) f_{FD}(E_i(k_i), E_{Fi}) [1 - f_{FD}(E_i(k_i), E_{Fi})]. \quad (12)$$

It was assumed that the distribution of electrons in each subband is a Fermi-Dirac distribution with the electron temperature equal to the lattice temperature, but with different Fermi levels for each subband ( $E_{Fi}$  for subband  $i$ ). Finally, we get an expression for the average transition rates  $W_{if} = \langle W_{if}^{LO-} \rangle + \langle W_{if}^{LO+} \rangle + \langle W_{if}^{A-} \rangle + \langle W_{if}^{A+} \rangle$ .

Equations (5)-(6), together with the condition  $n_s = n_1 + n_2 + n_3$  ( $n_s$  is the total electron density determined from electroneutrality of the structure), can be solved in the stationary case ( $\frac{d}{dt} = 0$ ) to find the electron densities in the subbands. Unfortunately, the transition rates, as we have seen, depend on the population of subbands, therefore a self-consistent treatment is necessary with an initial guess for the subband populations. The Fermi levels are then obtained from

$$E_{Fi} = E_{i0} + k_B T \ln \left( \exp \frac{\pi \hbar^2 n_i}{m_i k_B T} - 1 \right). \quad (13)$$

The transitions rates are then calculated according to (11)-(12) and the new electron densities are obtained from (5)-(6) and the electroneutrality condition. This step is repeated until the desired convergence is obtained. In our case, electron densities for the case of thermodynamic equilibrium are taken as a starting point for the self-consistent iteration and the procedure is repeated until the subband populations converge to within 1%.

Knowing the populations of the subbands it is easy to calculate the gain for stimulated emission, which is given by:

$$g = \sigma_{23} \frac{n_3 - n_2}{L_W}, \quad (14)$$

where  $\sigma_{23}$  is the lasing transition cross-section and  $L_W$  is the effective width of the quantum well structure.

### 3 Results

A range of double quantum wells with  $\text{Ga}_{1-x}\text{Al}_x\text{N}$  barriers with the same  $x$ , and GaN wells were investigated. The length of the outer barriers was set to a fixed value of 100 Å, while the inner barrier width  $L_b$ , left and right well widths  $L_{w1}$  and  $L_{w2}$ , and the AlN content in the barriers  $x$ , were varied.

Firstly,  $x$  was varied in the interval [0.1, 1] with a 0.1 step, and  $L_{w1}$ ,  $L_{w2}$  and  $L_b$  in the interval [10, 55] Å with a 5 Å step. We concluded that,

as one might have expected, for  $x \geq 0.2$  there are practically no structures with the desired spacings between the subbands  $E_{30} - E_{20} \approx 36$  meV and  $E_{20} - E_{10} \approx 91.2$  meV. At this point we can justify the assumption underlying equations (9) and (10). Since  $m_{GaN} = 0.20 m_0$ , and  $m_{AlN} = 0.30 m_0$ , for  $x \in [0, 0.2]$  the effective mass in the  $\text{Ga}_{1-x}\text{Al}_x\text{N}$  layer takes values from the interval  $[0.20 m_0, 0.22 m_0]$ . This means that its variation across the structure is small and therefore it may be considered almost constant, implying parabolic subbands with the same effective mass.

Secondly,  $x$  was varied in the interval  $[0.005, 0.200]$  with a 0.005 step, and  $L_{w1}$ ,  $L_{w2}$  and  $L_b$  in the interval  $[10, 95]$  Å with a 5 Å step. A range of structures having  $32 \text{ meV} \leq E_{30} - E_{20} \leq 40 \text{ meV}$  and  $83 \text{ meV} \leq E_{20} - E_{10} \leq 99 \text{ meV}$ , were chosen for further analysis. For all those structures, the modal gain defined as  $G_m = \sigma_{23}(n_3 - n_2)$  was calculated, with the desire to find the structure with the maximal modal gain. The calculation was performed at  $T = 77 \text{ K}$ , with a doping concentration ( $n_s = N_D L_W$ ) of  $N_D = 3 \times 10^{16} \text{ cm}^{-3}$ , while the pump flux was varied in the interval  $10^{21} - 10^{30} \text{ cm}^{-2}\text{s}^{-1}$  with one decade step. When the flux is less than  $10^{21} \text{ cm}^{-2}\text{s}^{-1}$ , none of the chosen structures had positive gain. At higher fluxes, the structure with  $x = 0.070$ ,  $L_{w1} = 90 \text{ Å}$ ,  $L_b = 15 \text{ Å}$ ,  $L_{w2} = 35 \text{ Å}$  is optimal in the range  $10^{22} - 10^{27} \text{ cm}^{-2}\text{s}^{-1}$  and was chosen for further analysis.

The profile of the conduction band edge of the chosen structure, as well as energy levels and the wave function moduli are given in figure 1.

Table 1 shows the values of the calculated average transition rates via interaction with LO and acoustic phonons for  $\Phi = 10^{27} \text{ cm}^{-2}\text{s}^{-1}$  and  $T = 77 \text{ K}$ . Our calculations show that these rates depend on the flux very weakly, meaning that these values can be considered as typical at  $T = 77 \text{ K}$ . It is interesting to note that for the  $3 \rightarrow 2$  transition the interaction with the acoustic phonon is dominant since the LO phonon emission is suppressed (the electron from the bottom of the third subband can not emit an LO phonon due to energy conservation).

$\langle W \rangle [\text{ps}^{-1}]$	$2 \rightarrow 1$	$3 \rightarrow 1$	$3 \rightarrow 2$
LO	15.64	16.43	0.0035
A	0.014	0.032	0.029
$\langle W \rangle [10^{-5} \text{ ps}^{-1}]$	$1 \rightarrow 2$	$1 \rightarrow 3$	$2 \rightarrow 3$
LO	0.73	0.0033	2.33
A	0.00061	0.0000077	13.2

Table 1:

Figure 3 shows the temperature dependence of the average transition



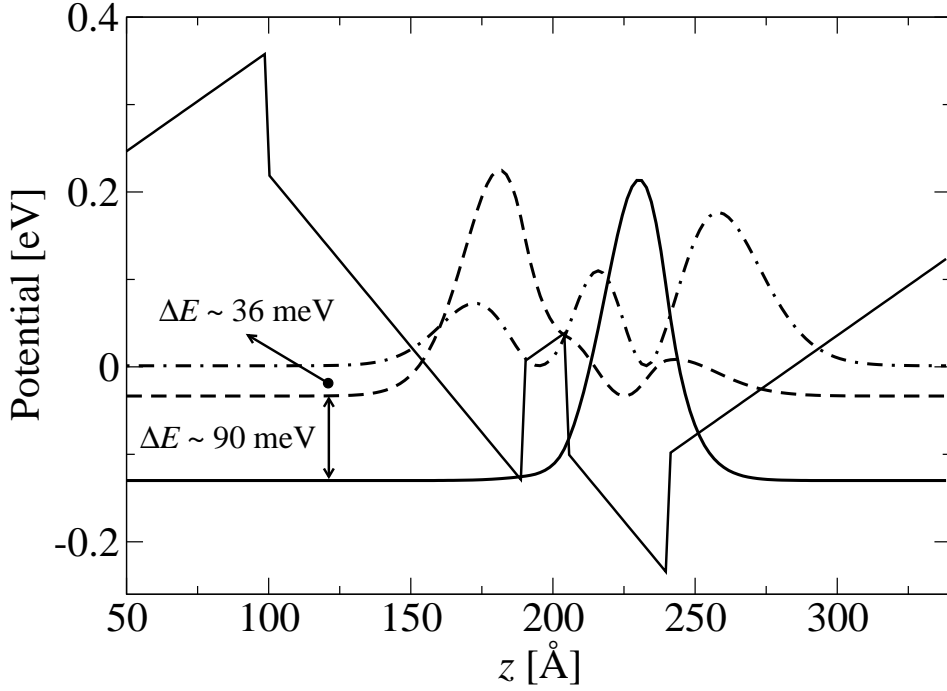


Figure 1:

rates from the higher to the lower subband. Transition rates from the lower to the higher subbands, not shown on the graph, grow significantly with temperature, since they are proportional to the number of phonons which also increases. Transition rate  $3 \rightarrow 2$  also rises with temperature. In the low temperature range this rise is mainly caused by the increase in number of acoustic phonons, while at higher temperatures it rises because the LO phonon emission rate becomes less suppressed. However, transition rates  $3 \rightarrow 1$  and  $2 \rightarrow 1$  don't increase with temperature, they even show a slight decrease. This is caused by the fact that the term  $N_0 + 1$  is practically constant with temperature, while at higher temperatures more electrons have higher in-plane wave vectors and thus slightly smaller transition rates.

The pumping flux dependence of the subband populations and gain is shown in figure 3. When the flux is low (around  $\Phi = 10^{21} \text{ cm}^{-2}\text{s}^{-1}$ )  $n_2$  is greater than  $n_3$  and there is no population inversion. At slightly higher flux (around  $\Phi = 10^{22} \text{ cm}^{-2}\text{s}^{-1}$ ) population inversion occurs. In the next part of the graph we see that  $n_3 \gg n_2$  and that  $n_3$  is linearly dependent on the flux. Finally, at  $\Phi \approx 10^{28} \text{ cm}^{-2}\text{s}^{-1}$ ,  $n_3$  approaches  $n_1$  and the graph reaches saturation. In the range from  $\Phi = 10^{23} \text{ cm}^{-2}\text{s}^{-1}$  to  $\Phi = 10^{27} \text{ cm}^{-2}\text{s}^{-1}$  the gain depends linearly on the flux, and then saturates (as well as  $n_3$ , this is

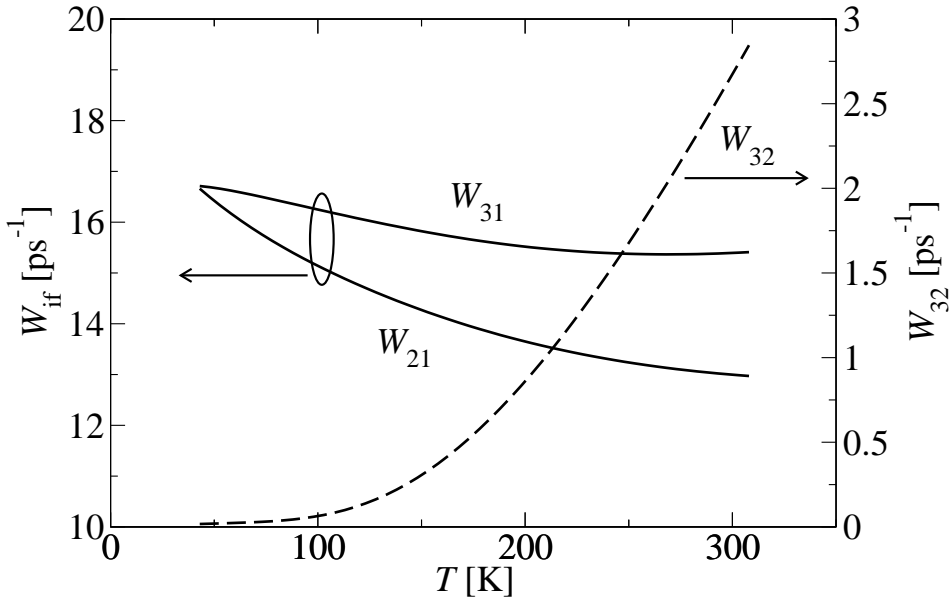


Figure 2:

expected since in that region  $n_3 \gg n_2$  so that gain is proportional to  $n_3$ ).

Figure 4 shows the temperature dependence of the electron densities and the gain. As expected, the gain decreases with temperature. However, as the LO phonon energy is considerably higher than the lasing energy, the undesirable LO phonon emission is suppressed resulting in only a slight decrease of the gain.

Finally, we discuss the possibility of the laser action by comparing the gain with estimated values of the waveguide losses. The waveguide design assumed here is based on a single-surface plasmon configuration with the gold top and highly doped thin GaN bottom contact layer, see Fig. 5, similar to that implemented in the recently reported terahertz QCLs[6]. To find the mode intensity pattern and the propagation losses we used a numerical calculation based on the transfer matrix method [21] with a wavelength dependent complex dielectric permittivity parameterized via the Drude model. We assumed the doping density of the  $0.15 \mu\text{m}$  thick bottom contact layer to be  $5 \times 10^{19} \text{ cm}^{-3}$  and around 130 periods of the designed optically pumped structure in the active region. The waveguide losses are calculated to be  $\alpha_W \approx 23 \text{ cm}^{-1}$  and the mode confinement  $\Gamma = 0.40$ . We have estimated the mirror losses, using  $\alpha_M = -1/(2L) \ln R$ , to be around  $2 \text{ cm}^{-1}$ , which gives the overall effective losses factor to be around  $(\alpha_W + \alpha_M)/\Gamma \approx 62 \text{ cm}^{-1}$ , less than the calculated gain for the pumping flux of  $\Phi = 10^{27} \text{ cm}^{-2}\text{s}^{-1}$ , even at room temperature (see Fig. 4).

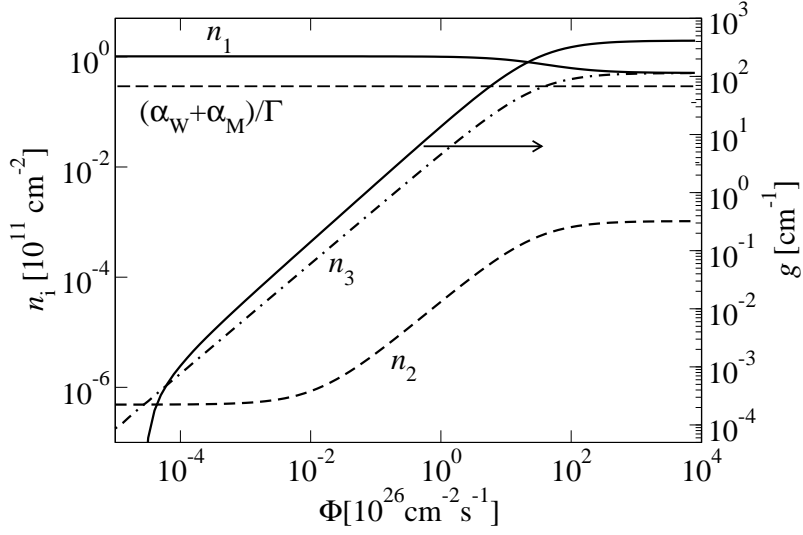


Figure 3:

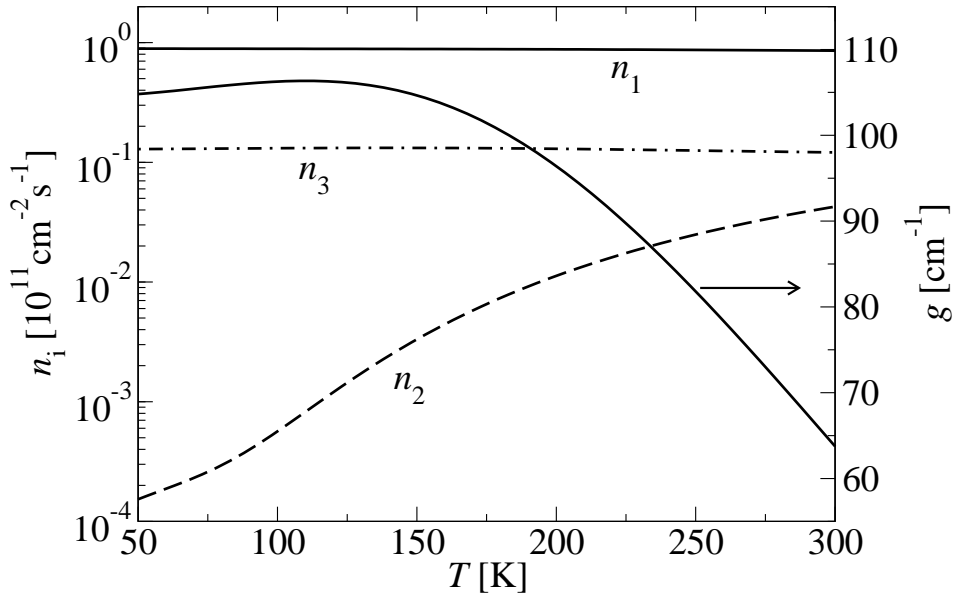


Figure 4:

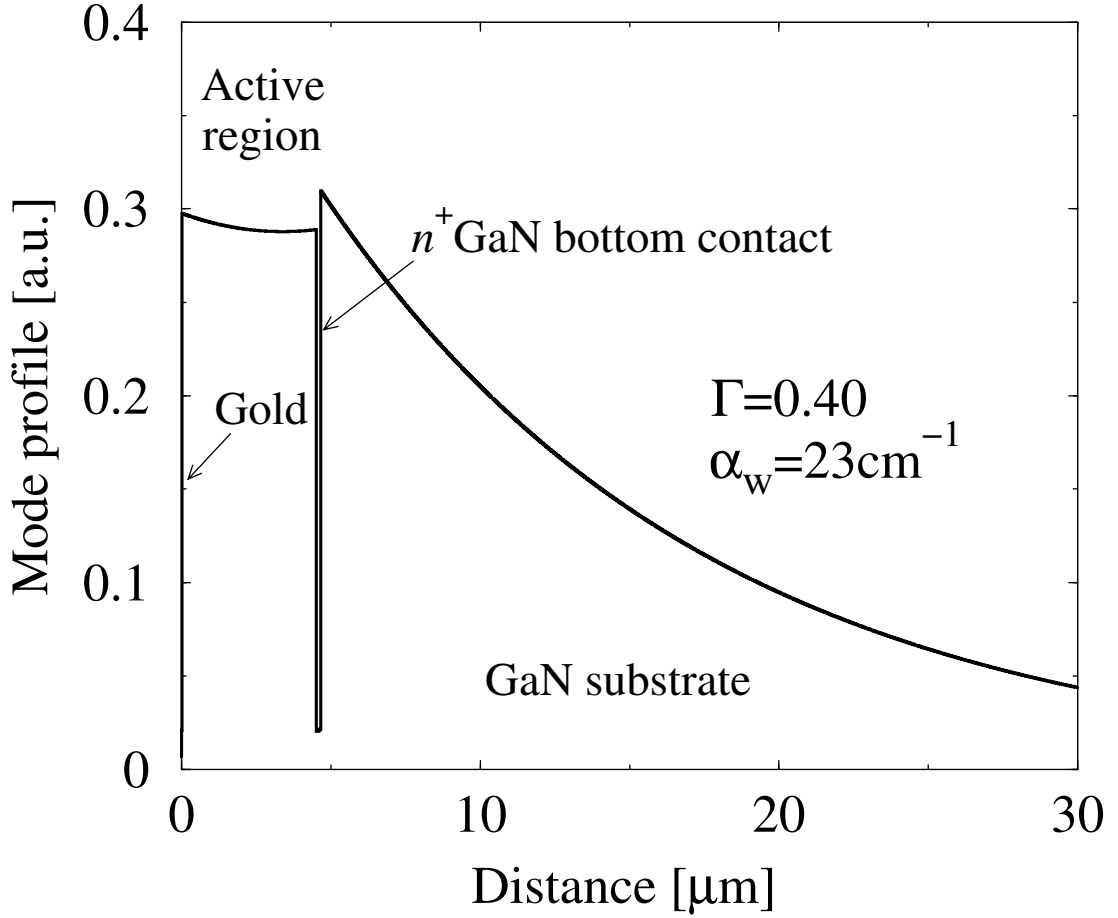


Figure 5:

## 4 Conclusion

In this paper, a prototype for an optically pumped intersubband THz laser emitting at  $\lambda \approx 34\mu\text{m}$  (36 meV i.e. in GaAs Reststrahlen region) based on a GaN/AlGaN double quantum well as an active region was proposed. The intersubband rate equations were solved self-consistently with both the LO and acoustic phonon transition rates taken into account. A design with the maximal modal gain among the investigated structures was selected for further analysis of flux and temperature dependence of gain. At  $T = 77\text{K}$  values of gain of around  $100\text{cm}^{-1}$  at flux of  $10^{27}\text{cm}^{-2}\text{s}^{-1}$  are predicted. A suitable waveguide design was presented, and losses and confinement factor calculated. For the designed structure the feasibility of lasing action even at room temperature is predicted by comparing the calculated modal gain with

estimated waveguide and mirror losses.

## References

- [1] R. F. Kazarinov and R. A. Suris, *Sov. Phys. Semicond.* **5**, 707 (1971).
- [2] J. Faist, F. Capasso, D. L. Sivco, C. Sirtori, A. L. Hutchinson, and A. Y. Cho, *Science* **264**, 553 (1994).
- [3] F. Capasso et al, *IEEE J. Quantum Electr.*, **38**, 511 (2002).
- [4] R. Köhler, A. Tredicucci, F. Beltram, H. E. Beer, E. H. Linfield, A. G. Davies, D. A. Ritchie, R. C. Iotti, F. Rossi, *Nature* **417**, 156 (2002).
- [5] B.S. Williams, S. Kumar, Q. Hu, and J. L. Reno, *Electr. Lett.* **40**, (2004).
- [6] G. Scalari, L. Ajili, J. Faist, H. Beere, E. Linfield, D. Ritchie, G. Davies, *Appl. Phys. Lett.* **82** 3165 (2003).
- [7] B.S. Williams, S. Kumar, H. Callebaut, Q. Hu, and J. L. Reno, *Appl. Phys. Lett.* **83**, 5142 (2003).
- [8] S. Kumar, B.S. Williams, S. Kohen, Q. Hu, and J. L. Reno, *Appl. Phys. Lett.* **84**, 2494 (2004).
- [9] S. Barbieri, J. Alton, H. E. Beer, J. Fowler, E. H. Linfield, and D. A. Ritchie, *Appl. Phys. Lett.* **85**, 1674 (2004).
- [10] O. Gauthier-Lafaye, P. Boucaud, F. H. Julien, S. Sauvage, S. Cabaret, J. M. Lourtios, V. Thierry-Mieg, and R. Planel, *Appl. Phys. Lett.* **71**, 3619 (1997).
- [11] N. Iizuka, K. Kaneko, N. Suzuki, T. Asano, S. Noda, and O. Wada, *Appl. Phys. Lett.* **77**, 648 (2000).
- [12] J. D. Heber, C. Gmachl, H. M. Ng, and A. Y. Cho, *Appl. Phys. Lett.* **81**, 1237 (2002).
- [13] C. Gmachl, S. V. Frolov, H. M. Ng, S.-N. G. Chu, and A. Y. Cho, *Electron. Lett.* **37**, 378 (2001).
- [14] D. Indjin, P. Harrison, R. W. Kelsall, Z. Ikonić, *Appl. Phys. Lett.*, **82**, 1347 (2003).
- [15] V. D. Jovanović, D. Indjin, Z. Ikonić, P. Harrison, *Appl. Phys. Lett.*, **84**, 2995 (2004).

- [16] V. Jovanović, Z. Ikonić, D. Indjin, P. Harrison, V. Milanović, and R. Soref, *J. Appl. Phys.* **93**, 3194 (2003).
- [17] F. Bernardini and V. Fiorentini, *Phys. Status Solidi B* **216**, 391 (1999).
- [18] I. Vurgaftman and J. R. Meyer, *J. Appl. Phys.* **94**, 3675 (2003).
- [19] M. Abramowitz and I. Stegun, *Handbook of Mathematical Functions* (Dover Publications, New York, 1965).
- [20] P. Harrison, *Quantum Wells, Wires and Dots*, John Wiley and Sons Ltd., Chichester, England, 2000.
- [21] E. Anemogiannis, E. N. Glytsis, T. K. Gaylord, *IEEE J. Lightwave Technol.* **17**, 929 (1999).

Figure captions

FIG. 1: Conduction band profile, energy levels and wave function moduli for the structure  $x = 0.070$ ,  $L_{w1} = 90 \text{ \AA}$ ,  $L_b = 15 \text{ \AA}$ ,  $L_{w2} = 35 \text{ \AA}$

FIG. 2: Temperature dependence of average transition rates at  $\Phi = 10^{27} \text{ cm}^{-2}\text{s}^{-1}$  for the structure from Fig. 1

FIG. 3: Flux dependence of electron densities (left axis), gain (right axis) and effective losses factor at  $T = 77 \text{ K}$  for the structure from Fig. 1

FIG. 4: Temperature dependence of electron densities and gain at  $\Phi = 10^{27} \text{ cm}^{-2}\text{s}^{-1}$  for the structure from Fig. 1

FIG 5: Single-plasmon waveguide design and mode profile. Total thickness of active region is  $4.5\mu\text{m}$  ( $\sim 130$  periods of structure). The  $0.15\mu\text{m}$  thick bottom contact layer is assumed to be doped with  $5 \times 10^{19}\text{cm}^{-3}$



Table caption

TABLE I: Average transition rates for interaction with longitudinal optical phonon (LO) and acoustic phonon (A) at  $\Phi = 10^{27} \text{ cm}^{-2}\text{s}^{-1}$  and  $T = 77 \text{ K}$